Molecular Dynamics Study of TiO_2/Poly(acrylic acid-*co*-methyl methacrylate) and Fe_3O_4/Polystyrene Composite Latex Particles Prepared by Heterocoagulation

Ying-Da Luo,[1] Jui-Hung Chen,[1] Ching-I Huang,[1] Wen-Yen Chiu[1–3]

[1]*Institute of Polymer Science and Engineering, National Taiwan University, Taipei, Taiwan, Republic of China*
[2]*Department of Chemical Engineering, National Taiwan University, Taipei, Taiwan, Republic of China*
[3]*Department of Material Science and Engineering, National Taiwan University, Taipei, Taiwan, Republic of China*

Received 8 January 2009; accepted 21 October 2009
DOI 10.1002/app.31652
Published online 14 January 2010 in Wiley InterScience (www.interscience.wiley.com).

ABSTRACT: All-atom molecular dynamics simulations were used to study the morphology of polymer/inorganic composite particles prepared by heterocoagulation. The results were also compared to those of our previous study of the preparation of TiO_2/poly(acrylic acid-*co*-methyl methacrylate) and Fe_3O_4/polystyrene composite particles. In the simulation system, polymer or inorganic particles were simulated by surface-charge-modified C_{60} or Na atoms. Through a combination of analysis of the radial distribution functions of charged atoms and snapshots of the equilibrated structure, three kinds of particle distributions were observed under different conditions. When the polymer and inorganic particles had opposite surface charges and their sizes were very different, the composite morphology showed a core–shell structure with small particles adsorbed onto the surfaces of large particles. Furthermore, when the polymer and inorganic particles had opposite surface charges but comparable sizes, the polymer and inorganic particles aggregated domain by domain. Finally, when the polymer and inorganic particles were endowed with the same surface charge, the distribution of these two types of particles was homogeneous, regardless of their size difference. The simulation results were in agreement with the experimental results. The electrostatic interaction and the size of the particles dominated the final morphology of the composite particles when the heterocoagulation method was used. © 2010 Wiley Periodicals, Inc. J Appl Polym Sci 116: 2275–2284, 2010

Key words: core–shell polymers; molecular dynamics; morphology; nanocomposites

INTRODUCTION

Heterocoagulation is the aggregation of two types of colloid particles that may differ in size, charge, or shape.[1] When two kinds of particles have opposite charges, these particles attract each other, and coagulation occurs. Therefore, it is a simple and useful method for fabricating composite particles. One can separately synthesize particles with opposite charges and create composite particles with a specific morphology, especially a core–shell morphology, by heterocoagulation. Studies of the kinetics of heterocoagulation and equilibrium morphologies of oppositely charged heterocoagulated polymeric colloids were started by Vincent and coworkers.[2–5] Later, Okubo and Lu[6] and Ottewill et al.[7] employed heterocoagulation of oppositely charged polymeric spheres to produce core–shell particles. Over the past several decades, the deposition of small latex particles onto larger, oppositely charged spherical latex particles has been reported extensively. Harley et al.[8] used a thin-film, freeze-drying/scanning electron microscopy technique to directly observe the adsorption of small colloidal particles onto larger colloidal particles of opposite charge. Adsorption isotherms were presented for small, negative latex particles adsorbed onto larger, positive latex particles at different electrolyte concentrations and in the presence and absence of pre-adsorbed layers of poly(vinyl alcohol-*co*-vinyl acetate) on both sets of particles. Serizawa et al.[9] studied the heterocoagulation of core–corona microspheres by means of electrostatic interactions with respect to the effects of the particle size and mixture ratios. Polystyrene (PS) microspheres with poly(vinyl amine) and poly(methacrylic acid) coronas were synthesized and used as cationically and anionically charged microspheres, respectively. Although the concepts and applications of heterocoagulation are well known in the literature, there has been no research exploring such phenomenon on the atomic scale.

All-atom molecular dynamics simulations analyze the force field between atoms to calculate the

Correspondence to: W.-Y. Chiu (ycchiu@ccms.ntu.edu.tw).

interaction between all molecules and predict the site of molecules in the next moment. This gained great popularity in materials science first and then was extended to biochemistry and biophysics[10] in the 1970s. Brown et al.[11] investigated the effect of the filler particle size on the properties of a model nanocomposite. Karami et al.[12] studied the hydrogen-bond dynamics of polyamide 66 over a broad temperature range (300–600 K). Gertner and Hynes[13] studied the acid ionization of hydrochloric acid (HCl) at the basal plane surface of ice at 190 K. Ju et al.[14] studied a single chain of poly(methacrylic acid) in aqueous solutions at various degrees of charge density via all-atom molecular dynamics simulations. In the study of Li et al.,[15] the glass-transition temperature of an aqueous glycerol solution (60 wt %) was determined by isothermal–isobaric molecular dynamics simulation (constant pressure and temperature molecular dynamics). The glass-transition temperature values determined by the simulation method were compared with the values in the literature.

Until now, there have been few articles discussing the effect of the particle size or the charges of particles on the heterocoagulation process in both experiments and dynamic simulations. Brownian dynamic simulations of heterocoagulated composites were studied by some researchers.[16] However, the force field in the Brownian model is more simplified in comparison with the all-atom molecular dynamics model. Although the simulation time can be shortened in the Brownian model, the accuracy of the simulation results may be influenced. In this research, an all-atom molecular dynamics simulation was employed to simulate the morphology of composite particles, and it was compared with the heterocoagulation experiments of our previous work on the production of TiO_2/poly(acrylic acid-*co*-methyl methacrylate) [P(AA-*co*-MMA)][17] and Fe_3O_4/PS for the first time. The radial distribution function (RDF) profiles of the charged atoms and the snapshots of the simulation system were traced to investigate the distributions of the composite particles. The effects of the charge and size of the inorganic and latex particles on the morphology of the composite particles were also discussed and verified via both experiments and simulations.

EXPERIMENTAL

Materials

Titanium tetraisopropoxide was used to prepare TiO_2 inorganic particles. Iron(II) chloride tetrahydrate and iron(III) chloride hexahydrate were used to prepare Fe_3O_4 inorganic particles. Lauric acid was used to modify the surface of Fe_3O_4 particles. Acrylic acid and methyl methacrylate were used to synthesize P(AA-*co*-MMA) latexes; this was initiated by 2,2-azobis(isobutyramidine) dihydrochloride or potassium persulfate (KPS). Styrene was used to synthesize PS latices; this was initiated by 2,2′-azobisisobutylonitrile. Sodium dodecyl sulfate (SDS) and cetyltrimethylammonium chloride (CTAC) were used as anionic and cationic surfactants, respectively. All the chemicals mentioned previously were purchased from Acros (Geel, Belgium) and used as supplied. Deionized water was used throughout the work.

Preparation of the TiO_2/latex composite particles

The TiO_2 dispersion and soapless, anionic, and cationic P(AA-*co*-MMA) latexes were prepared first. The anionic and cationic P(AA-*co*-MMA) latexes were produced with the surfactants SDS and CTAC, respectively. The soapless P(AA-*co*-MMA) latex was stabilized with the charged initiator KPS. The preparation procedure is described in detail in our previous study.[17] Each of these three different copolymer latexes was mixed with the TiO_2 dispersion at a weight ratio of 1 : 1, 2 : 8, or 3 : 7. However, only the data for the 1 : 1 case are reported in this article. All composites were prepared by the addition of the dialyzed copolymer latex to the TiO_2 dispersion drop by drop with stirring for 1 h at room temperature. When the copolymer latex was added to the TiO_2 dispersion, the inorganic and organic components combined to form precipitates quickly. The precipitates were washed with water and then separated from the dispersion supernatant by centrifugation at 8000 rpm for 10 min repeatedly to remove the free nanoparticles, and they were dried in a vacuum oven.

Preparation of the Fe_3O_4/latex composite particles

The Fe_3O_4 dispersion was prepared by a coprecipitation method followed by a surface treatment of the surfactant double layers.[18] The first layer was lauric acid, and its carboxylic acid group was anchored on the iron atom.[19] Then, the hydrophobic interaction between lauric acid and SDS formed the second surfactant layer. The anionic and cationic PS latexes were prepared by miniemulsion polymerization with the anionic surfactant SDS or the cationic surfactant CTAC. All composites were prepared by the addition of the Fe_3O_4 dispersion to the PS latex particles drop by drop with stirring for 1 h at room temperature. The Fe_3O_4/PS weight ratio was about 20%. Finally, the composite latex was dropped onto the surface of the copper grid for transmission electron microscopy (TEM) observation. It is worth mentioning that when two kinds of particles are mixed to form composite particles, the addition of the

(a)

$$E = \sum E^b + \sum E^a + \sum E^0 + \sum E^t + \sum E^{bb} + \sum E^{ab} + \sum E^{aa} + \sum E^{at} + \sum E^{bt} + \sum E^{elec} + \sum E^{VDW}$$

E^b : Energy from distortion of bond length
E^a : Energy from distortion of bond angle
E^0 : Energy from distortion of out-of-plane bending angle
E^t : Energy from distortion of torsion angle
E^{bb} : Energy from the cross term between two bonds
E^{ab} : Energy from the coupling between a bond and an angle
E^{aa} : Energy from two angles with a common bond
E^{at} : Energy from an angle and torsion
E^{bt} : Energy from interaction between a bond and dihedral angle of rotation
E^{elec} : Energy from electrostatic interaction
E^{VDW} : Energy from van der Waals interaction

(b)

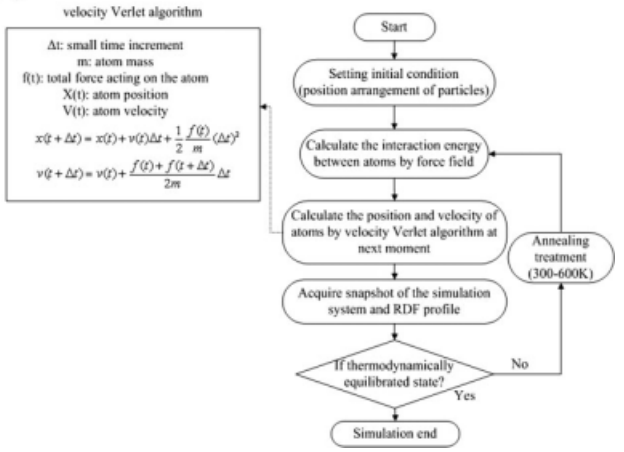

Scheme 1 (a) Total potential energy of the force field used in the simulation system[21] and (b) flow chart of the simulation process.

minor particles (small in amount) to the major particles (large in amount) will enhance the efficiency of mixing. This explains our choice of different addition orders for preparing Fe_3O_4/latex and TiO_2/latex composite particles.

Model and simulation method

An energy calculation and dynamics simulation program was employed;[20] this was an all-atom model used to calculate the atomic interaction parameters between the latex particles. The total potential energy function was composed of the bonded interaction and nonbonded interaction. The bonded interaction was contributed by bond stretching, bond angle bending, and torsion angle twisting mainly. The nonbonded interaction included the van der Waals force and electrostatic Coulomb potential energy.[21] The potential energy function is exhibited in detail in Scheme 1. The Forcite module of Material Studio molecular modeling software was used to construct the atomic structure for further molecular dynamics simulation in this research. A fullerene structure (C_{60}) with a diameter of 0.7 nm[22] or a sodium atom with a diameter of 0.168 nm[23] was established as the basis for simulating the polymer latex particles or inorganic particles. The selection of the C_{60} structure for the particles was due to its spherical shape with a minimized atom number. This can greatly reduce the computation time of dynamic modeling. For the C_{60} structure, the OSO_3 group was bonded to all 60 carbon atoms of C_{60} to provide the surface charges, as presented in Figure 1. The location of the charged atoms is indicated by black. The chemical structure of the OSO_3 group is shown in Figure 1(b), in which the charged (+1 or −1) atom is marked with an asterisk to simulate a particle with positive or negative charges. Meanwhile, the sodium atom was assigned a charge of +1 or −1 to simulate a small particle with positive or negative charges. The counter ions and water molecules were not taken into account in the simulation to simplify the computation. The molecular dynamics simulations were performed by integration over the positions and velocities of all atoms according to the velocity Verlet algorithm.[24,25] Several charged particles were first put in a vacuum box with a side length of 100 Å and a periodic boundary condition. The Ewald summation method was used for the calculation of the interaction energies for periodic systems.[26] Before simulation, the conjugated gradient minimization method was adopted to relax and equilibrate the initial structure. Then, an annealing process was used to accelerate the achievement of the equilibrated state. The annealing temperature was first raised from 300 to 600 K in 5 ps and cooled to 300 K in another 5 ps; this was called one annealing cycle. The annealing cycle was repeated at least five times to ensure that the system had been equilibrated. After these processes were performed so that the system energy had reached the equilibrium value, the RDFs at different times during the process of annealing were analyzed. This RDF [$g_{A-B}(r)$] indicates the average local probability density of finding

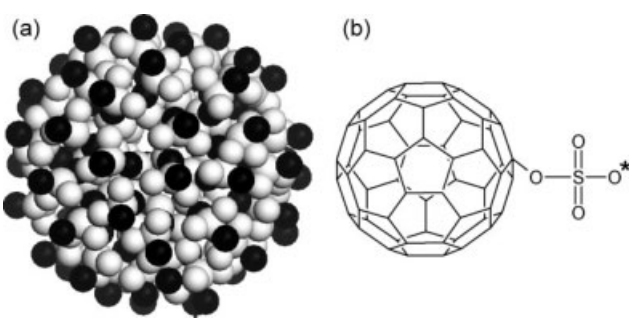

Figure 1 (a) Schematic presentation of the charged C_{60} structure; the charged atoms are shown in black. (b) Chemical structure of the charged OSO_3 group; the charged atoms are marked with an asterisk.

TABLE I
Size and ζ Potential of the Synthesized Inorganic Particles and Latex Particles

	Particle size (nm)	ζ potential (mV)
TiO_2[a]	12.4	53.6
Soapless P(AA-*co*-MMA) latex[a]	180	−33.9
Anionic P(AA-*co*-MMA) latex[a]	32.7	−31.1
Cationic P(AA-*co*-MMA) latex[a]	20	19.9
Fe_3O_4	8	Negative
Anionic PS latex	175	Negative
Cationic PS latex	180	Positive

[a] These data were taken from ref. 17.

B atoms at distance *r* from *A* atoms over the equilibrium density:

$$g_{A-B}(r) = \frac{n_B/4\pi r^2 dr}{N_B/V} \quad (1)$$

where n_B is the number of *B* atoms at distance *r* in a shell of thickness *dr* from atom *A*, N_B is the total number of *B* atoms in the system, and *V* is the total volume of the system. The flowchart of the simulation process is drawn in Scheme 1. It is worth mentioning that although the diameters of the simulation particles were different from those of the inorganic and polymer particles in experiments, the diameter ratio of the simulation particles was controlled to be similar to the corresponding experimental particles. For example, in the simulation system with various particle sizes, the size of the large particles (OSO_3^--capped C_{60}) was about 1.4 nm. It was almost 10 times the size (0.168 nm) of the small particles (Na^{+1} atoms). In the experimental system, the size ratio of the large polymer particles to inorganic particles ranged from 10 to 20 according to the size data in Table I. On the other hand, when the simulation system with the same particle size was used, the diameter ratio of the experimental polymer particles to the inorganic particles ranged from 1.5 to 2.5. It was hard to design a particle size exactly the same as the experimental particle size in our simulation systems, but the simulation results were reasonable when the difference in the size ratios of the experiments and simulation systems was not larger than an order of magnitude.

RESULTS AND DISCUSSION

Morphology of the composite latex particles from the experiments

In the experiments, TiO_2/P(AA-*co*-MMA) and Fe_3O_4/PS composite latex particles were prepared by heterocoagulation. The sizes and ζ potentials of the synthesized inorganic particles and polymer latex particles are shown in Table I. The positive charge of TiO_2 was due to the fact that the pH value was controlled below its isoelectric point. The negative charge of Fe_3O_4 came from the anionic surfactant treatment of the particle surface. For the soapless polymer latex, negative charges resulted from the negatively charged radicals ($SO_4^{-2}{}_*$) from the initiator KPS. For the anionic polymer latex, negative charges were contributed not only by the initiator but mostly by the negatively charged surfactant SDS. For the cationic latex, positive charges resulted from the positively charged surfactant CTAC. In the case of TiO_2 composite latex particles, SEM pictures of the burned and precipitated TiO_2/soapless latex composite, TiO_2/anionic latex composite, and TiO_2/cationic latex composite are shown in Figure 2. Through burning of the TiO_2/latex composite at 500°C to remove the polymer component, we could observe the distribution of inorganic and organic components in the TiO_2/latex composite from the residual morphology. The dark regions and white regions represent the polymer and TiO_2, respectively. Here we assumed that after it was burned at 500°C, almost no organic components were present, and only inorganic components were left. In the SEM image of the TiO_2/cationic latex composite exhibited in Figure 2(c), small white particles, regarded as TiO_2 particles, showed a homogeneous distribution with no obvious aggregation. On the other hand, in Figure 2(a), large aggregations of TiO_2 particles in the range of 200–300 nm, which was about the size of the soapless latex particles, were apparent in the SEM image of the TiO_2/soapless latex composite, whereas the morphology of the TiO_2/anionic latex complex showed less aggregation than the TiO_2/soapless latex composite in Figure 2(b). Instead, domain-by-domain aggregation was observed. In the case of the Fe_3O_4 composite latex particles, TEM images of the Fe_3O_4/anionic latex composite and Fe_3O_4/cationic latex composite are shown in Figure 3(a,b), respectively. The Fe_3O_4/anionic latex composite demonstrated a random distribution between polymer and inorganic particles. However, when the latex particles were positively charged, the morphology of the Fe_3O_4/cationic latex composite exhibited an obvious core–shell structure. All the Fe_3O_4 nanoparticles covered the surface of the PS particles, as shown in Figure 3(b). On the basis of the experimental results shown in Figures 2 and 3, it could be concluded that the electrostatic force and the size difference between the polymer and inorganic particles were responsible for the final morphology of the composite particles. The results were investigated by molecular dynamics simulation too.

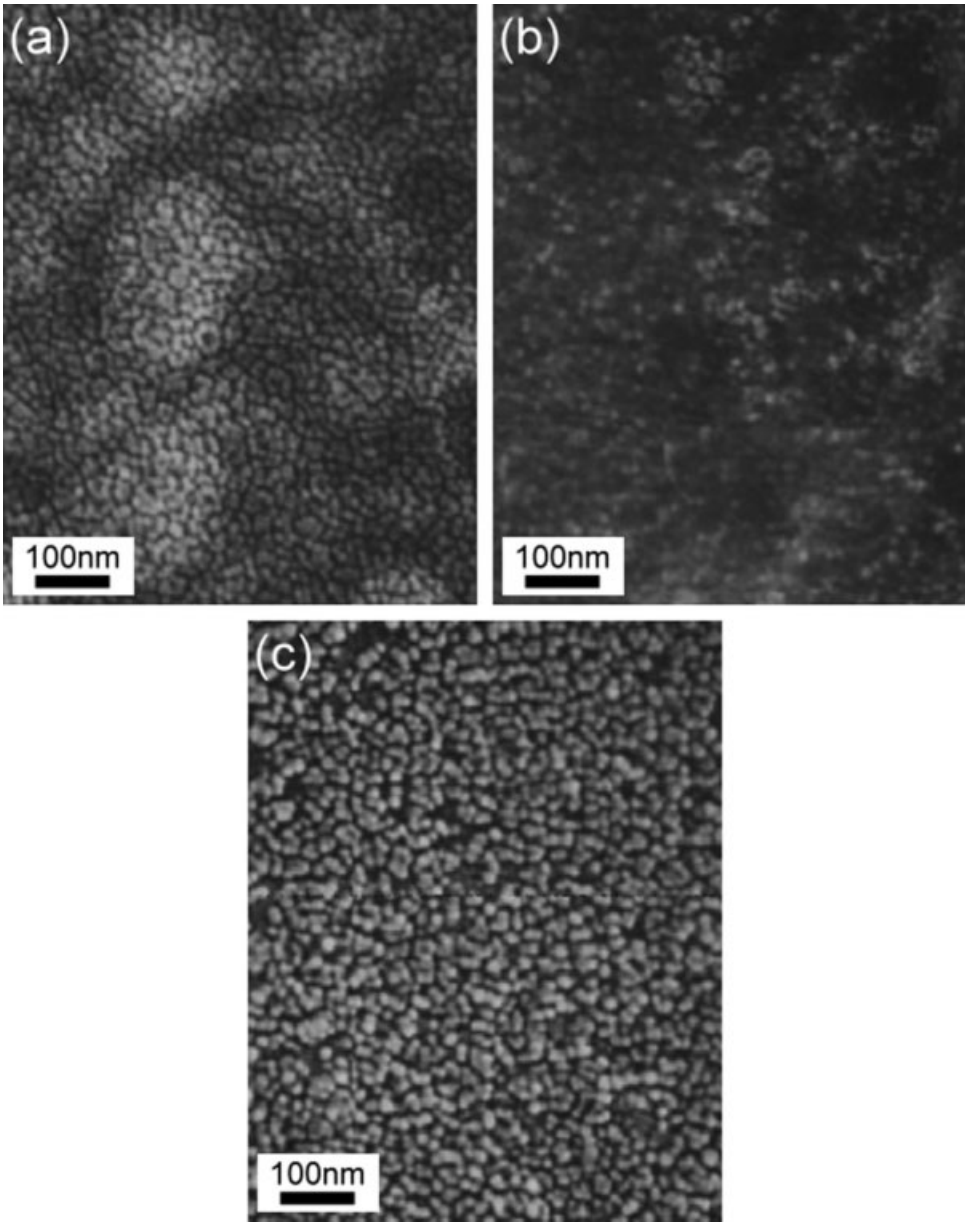

Figure 2 SEM of burned (a) TiO_2/soapless latex, (b) TiO_2/anionic latex, and (c) TiO_2/cationic latex.

Morphology of the composite latex particles from the simulation: Different sizes and different charge polarities

In this system, 14 large particles (black balls) with negative charges and 140 small particles (gray balls) with positive charges were established in the box first. The large particles were presented by OSO_3^--capped C_{60} to simulate the polymer latex particles. The small particles were set with Na^{+1} atoms to simulate the inorganic particles. Initially, these two kinds of particles were randomly put into the box. The arrangement of all particles in the initial state is shown in Figure 4(a). The homogeneous distribution between large and small particles can be verified by the RDF profile of charged Na^{+1} atoms of small particles with respect to the O^{-1} atoms of large particles in Figure 5. No prominent peak with an intensity higher than 1 was observed in the RDF profile initially. This indicated that the local probability density of finding charged Na^{+1} atoms near O^{-1} atoms was quite even. The onset value of the RDF profile was about 12 Å (Fig. 5). This revealed that there was no possibility of finding an Na^{+1} atom within a 12-Å distance from an O^{-1} atom initially. However, when the simulation system underwent an annealing treatment for 25 ps, a peak at 3 Å appeared. The result implied that there was an interaction between the large particles and small particles. When the annealing time was increased from 25 to 100 and 150 ps, the intensity of the prominent peak increased from

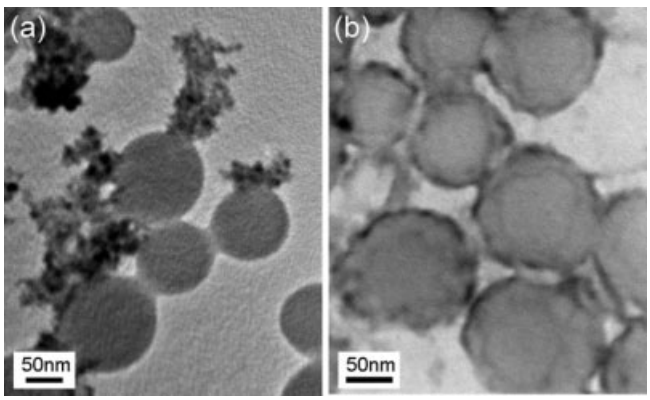

Figure 3 TEM of (a) Fe_3O_4/anionic latex and (b) Fe_3O_4/cationic latex.

15 to a steady value of 30. The results showed that more and more small particles interacted with large particles. According to the snapshots of the simulation system, the number of small particles that adsorbed onto the surface of large particles increased with time, and this was consistent with the RDF results. Finally, all small particles were located on the surface of large particles, as shown in Figure 4(b), when the equilibrated structure was achieved.

The simulation results were in agreement with our experimental results. The TiO_2 particles with a positive ζ potential were adsorbed onto the surface of soapless latex particles with a negative ζ potential [Fig. 2(a)]. The Fe_3O_4 particles with negative charges were located on the shell layer of cationic latex particles [Fig. 3(b)]. The driving force of this core–shell morphology came from the electrostatic attraction force between inorganic particles and polymer latex particles.

Morphology of the composite latex particles from the simulation: Same size and different charge polarities

In this system, 13 particles (black balls) with negative charges and 14 particles (gray balls) with positive charges were established in the box first. The black balls were charged by OSO_3^--capped C_{60} to simulate the anionic P(MMA-*co*-AA) latex particles. The gray balls were set with OSO_3^+-capped C_{60} to simulate the TiO_2 particles. Hence, the sizes of the positive particles and negative particles were similar. Initially, these two kinds of particles were randomly put into the box. The arrangement of the particles in the initial state is shown in Figure 6(a). The homogeneous distribution between gray and black balls could be verified by the RDF profile of the O^{+1} atom of the gray ball with respect to the O^{-1} atom of the black ball in Figure 7. No prominent peak with an intensity higher than 1 was observed in the RDF profile. This indicated that the local probability density of finding charged O^{+1} atoms near O^{-1} atoms was quite even initially. The onset value of the RDF profile was about 12 Å. This revealed that there was no possibility of finding an O^{+1} atom within a 12-Å distance from an O^{-1} atom initially. However, when the simulation system underwent an annealing treatment for 3 ps, the local probability density increased to about 2. This indicated that certain O^{+1} and O^{-1} atoms attracted each other. When the annealing time was increased to 25 ps, the prominent peak at 2 Å appeared. Meanwhile, several other peaks at 5, 11, and 15 Å appeared. Each particle had 60 atoms with positive or negative charges. The prominent peak indicated the nearest distance between O^{+1} and O^{-1} atoms, and the other peaks indicated the distances of O^{+1} atoms in gray balls with respect to the other O^{-1} atoms in the neighboring gray balls. According

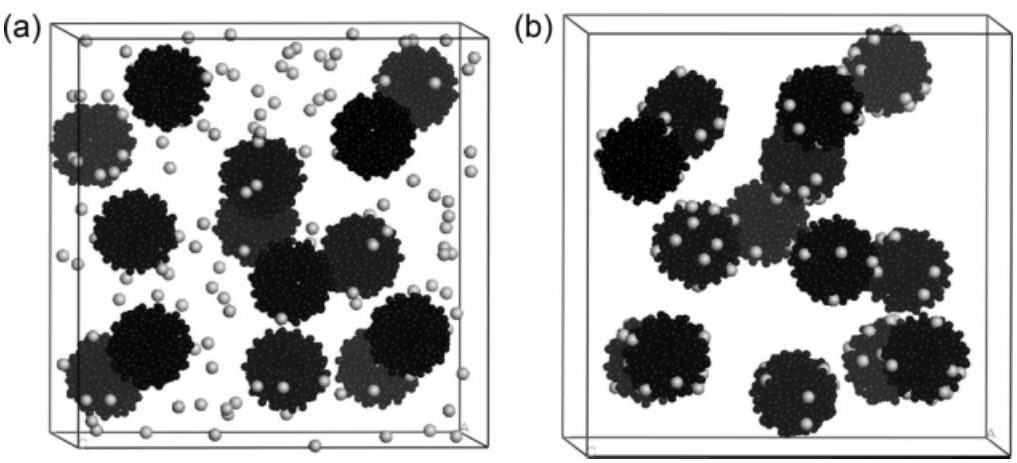

Figure 4 Snapshots of the simulation system of the TiO_2/soapless and Fe_3O_4/cationic latices: (a) initial state and (b) equilibrated state. The soapless latex and TiO_2 particles are shown by black and gray balls, respectively.

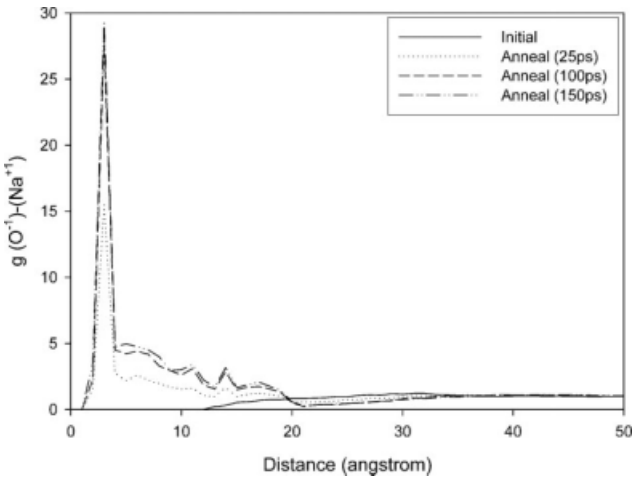

Figure 5 RDFs of the Na^{+1} atom of the gray balls with respect to the O^{-1} atom of the black balls at various annealing times.

to the snapshot of the equilibrated simulation system in Figure 6(b), the black balls and gray balls aggregated in domains. This was consistent with our RDF results. The simulation results could be compared with our experimental results. The TiO_2 particles with a positive ζ potential and anionic latex particles with a negative ζ potential aggregated domain by domain [Fig. 2(b)], and the sizes of the TiO_2 and anionic latex particles were comparable. The simulation results conformed well with the experiments.

Morphology of the composite latex particles from the simulation: Same size and same charge polarity

In this system, 14 particles (black balls) with positive charges and 13 particles (gray balls) with positive charges were established in the box first. The black and gray balls were all presented by OSO_3^+-capped C_{60} to simulate the cationic P(MMA-*co*-AA) latex and TiO_2 particles, respectively. The sizes of the black and gray balls were the same. Initially, these two kinds of particles were put into the box. The arrangement of the particles in the initial state is shown in Figure 8(a). The O^{+1} atoms of gray balls were put close to the O^{+1} atoms of black balls initially, and this resulted in the higher average local probability density at a distance of 20 Å in the initial RDF profile in Figure 9. However, when the simulation system underwent an annealing treatment for 5 ps, the local probability density decreased to a steady value of about 1. This indicated that the O^{+1} atoms in a single particle repulsed other charged particles and attained a homogeneous distribution. As the annealing time was increased from 25 to 50 ps, there was no significant change in the snapshot or RDF profile of the simulation system. This implied that the system had reached a thermodynamically equilibrated state. The snapshot of the equilibrated simulation system is shown in Figure 8(b). The black balls and gray balls demonstrated a homogeneous distribution. This could be attributed to the electrostatic repulsion force between particles. The snapshot picture is also in agreement with the experimental SEM photograph in Figure 2(c).

Morphology of the composite latex particles from the simulation: Different sizes and the same charge polarity

In this system, 14 large particles (black balls) with negative charges and 140 small particles (gray balls) with negative charges were established in the box first. The large particles were presented by OSO_3^--capped C_{60} to simulate the polymer latex particles (anionic PS latex). The small particles were set with Na^{-1} atoms to simulate the inorganic particles (Fe_3O_4). Initially, these two kinds of particles were randomly put into the box. The arrangement of the

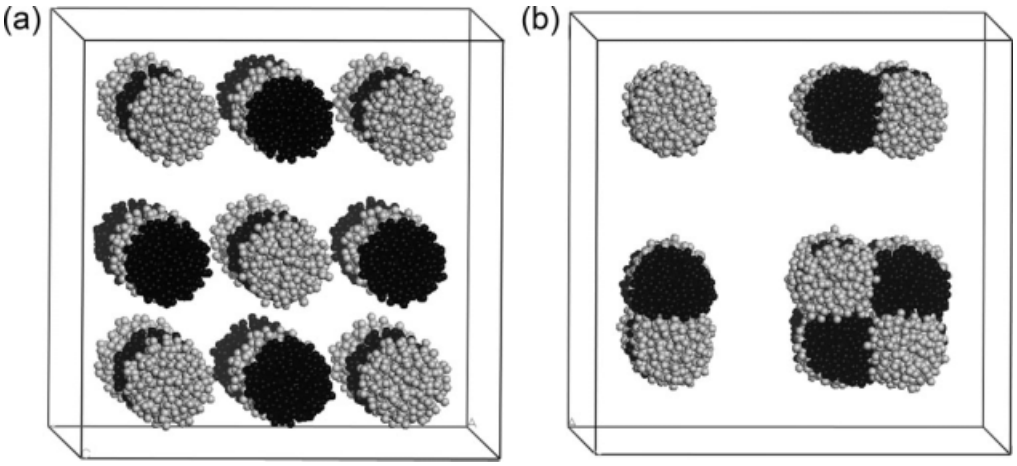

Figure 6 Snapshots of the simulation system of the TiO_2/anionic latex: (a) initial state and (b) equilibrated state. The anionic latex and TiO_2 particles are shown by black and gray balls, respectively.

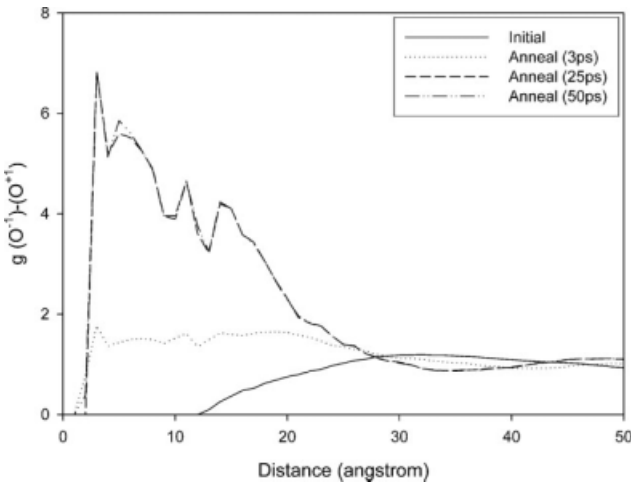

Figure 7 RDFs of the O^{+1} atom of the gray balls with respect to the O^{-1} atom of the black balls at various annealing times.

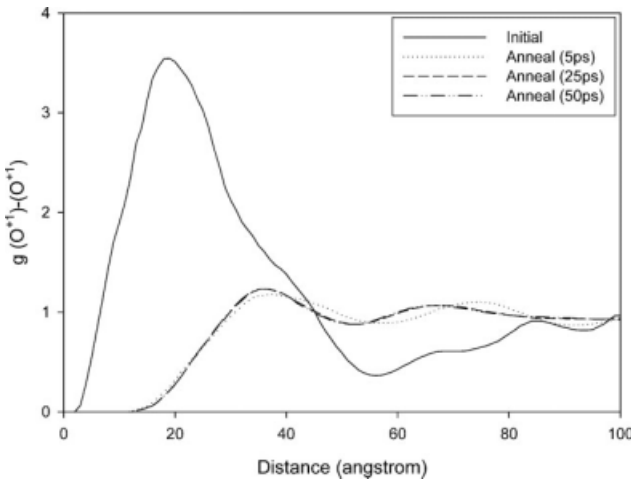

Figure 9 RDFs of the O^{+1} atom of the gray balls with respect to the O^{+1} atom of the black balls at various annealing times.

particles in the initial state is shown in Figure 10(a). From the RDF profile in Figure 11, the Na^{-1} atoms of gray balls with respect to the O^{-1} atoms of black balls displayed a homogeneous distribution initially. As the annealing time was increased from 50 to 100 ps, there was no significant change in the snapshot or RDF profile of the simulation system. This implied that the system had reached a thermodynamically equilibrated state. The snapshot of the equilibrated simulation system is shown in Figure 10(b). The black balls and gray balls retained a homogeneous distribution. This was attributed to the electrostatic repulsion force between the polymer and inorganic particles. The results are in agreement with the experimental TEM photograph in Figure 3(a).

CONCLUSIONS

All-atom molecular dynamics simulations were applied to investigate the effects of the surface charge and size of polymer and inorganic particles on the morphology of mixtures of these particles. The simulation results were compared with our experiments. When the particles of the simulation system were set with different sizes and different charge polarities, the snapshot of the simulation system and RDF of the charged atoms showed a strong electrostatic attraction force between these two kinds of particles. The small particles were all adsorbed onto the surface of the large particles. The results were in agreement with our experimental results for TiO_2/soapless and Fe_3O_4/cationic composite latices via heterocoagulation. The aggregation size of the inorganic particles was close to the size of the

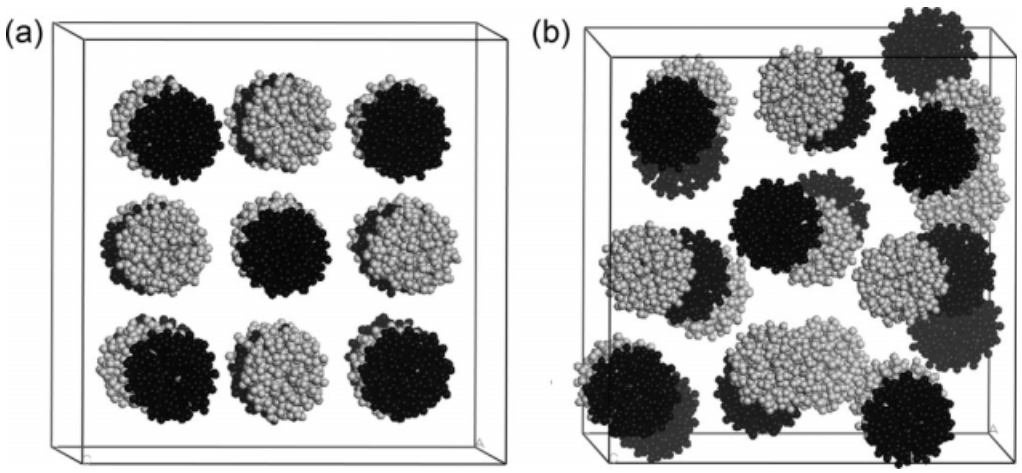

Figure 8 Snapshots of the simulation system of the TiO_2/cationic latex: (a) initial state and (b) equilibrated state. The cationic latex and TiO_2 particles are shown by black and gray balls, respectively.

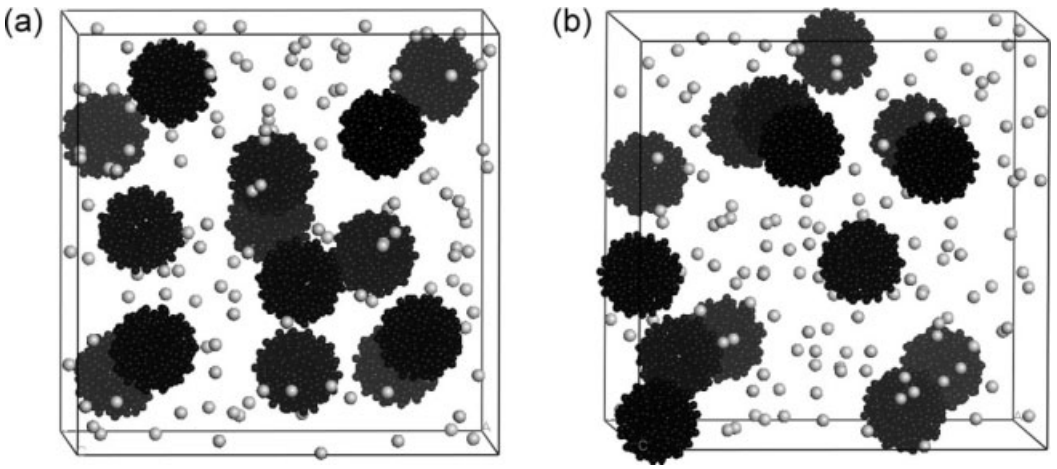

Figure 10 Snapshots of the simulation system of the Fe_3O_4/anionic latex: (a) initial state and (b) equilibrated state. The anionic latex and Fe_3O_4 particles are shown by black and gray balls, respectively.

polymer latex particles after part of the polymer was burned. However, when the sizes of the polymer and inorganic particles were close, the attraction force remained, but local aggregation was observed domain by domain. This could be compared to our SEM photograph of the burned TiO_2/anionic latex composite. Finally, as long as the surface charges of the particles were the same, the snapshot of the equilibrated simulation system showed a homogeneous distribution, and the RDF profile had a steady value of about 1; the size of the inorganic and polymer particles did not influence the morphology. This explained the SEM photograph of the TiO_2/cationic latex composite and the TEM photograph of the Fe_3O_4/anionic latex composite. In all, the molecular dynamics simulation indicated that the morphology of the polymer/inorganic composite latex was strongly influenced by the charge polarity and particle size. When the polymer and inorganic particles were very different in size and bore opposite surface charges, uniform core–shell composite particles could be successfully prepared with a heterocoagulation process.

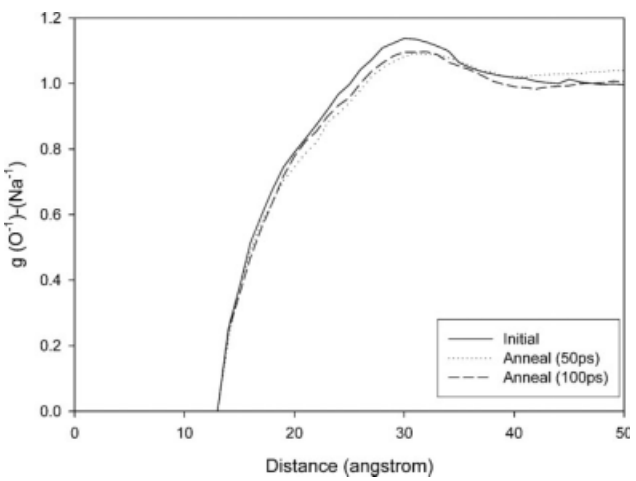

Figure 11 RDFs of the Na^{-1} atom of the gray balls with respect to the O^{-1} atom of the black balls at various annealing times.

The authors appreciate Yi-Kang Lan and Yong-Ting Chung for their help with the molecular dynamics simulation.

References

1. Islam, A. M.; Chowdhry, B. Z.; Snowden, M. J. Adv Colloid Interface Sci 1995, 62, 109.
2. Vincent, B.; Young, C. A.; Tadros, T. F. Faraday Discuss Chem Soc 1978, 65, 296.
3. Vincent, B.; Young, C. A.; Tadros, T. F. J Chem Soc Faraday Trans 1 1980, 76, 665.
4. Vincent, B.; Jafelicci, M.; Luckham, P. F.; Tadros, T. F. J Chem Soc Faraday Trans 1 1980, 76, 674.
5. Luckham, P.; Vincent, B.; Hart, C. A.; Tadros, T. F. Colloids Surf 1980, 1, 281.
6. Okubo, M.; Lu, Y. Colloids Surf A 1996, 109, 49.
7. Ottewill, R. H.; Schofield, A. B.; Waters, J. A.; Williams, N. S. J. Colloid Polym Sci 1997, 275, 274.
8. Harley, S.; Thompson, D. W.; Vincent, B. Colloids Surf 1992, 62, 153.
9. Serizawa, T.; Taniguchi, K.; Akashi, M. Colloids Surf A 2000, 169, 95.
10. Karplus, M.; McCammon, J. A. Nat Struct Biol 2002, 9, 646.
11. Brown, D.; Marcadon, V.; Mele, P.; Alberola, N. D. Macromolecules 2008, 41, 1499.
12. Karimi-Varzaneh, H. A.; Carbone, P.; Muller-Plathe, F. Macromolecules 2008, 41, 7211.
13. Gertner, B. J.; Hynes, J. T. Science 1996, 271, 1563.
14. Ju, S. P.; Lee, W. J.; Huang, C. I.; Cheng, W. Z.; Chung, Y. T. J Chem Phys 2007, 126, 10.
15. Li, D. X.; Liu, B. L.; Liu, Y. S.; Chen, C. L. Cryobiology 2008, 56, 114.
16. Puertas, A. M.; Maroto, J. A.; Barbero, A. F.; de las Nieves, F. J. Phys Rev E 1999, 59, 1943.

17. Chen, J. H.; Dai, C. A.; Chen, H. J.; Chien, P. C.; Chiu, W. Y. J Colloid Interface Sci 2007, 308, 81.
18. Wooding, A.; Kilner, M.; Lambrick, D. B. J Colloid Interface Sci 1991, 144, 236.
19. Kataby, G.; Cojocaru, M.; Prozorov, R.; Gedanken, A. Langmuir 1999, 15, 1703.
20. Levitt, M.; Hirshberg, M.; Sharon, R.; Daggett, V. Comput Phys Commun 1995, 91, 215.
21. Sun, H.; Mumby, S. J.; Maple, J. R.; Hagler, A. T. J Am Chem Soc 1994, 116, 2978.
22. Lang, H. P.; Thommengeiser, V.; Bolm, C.; Felder, M.; Frommer, J.; Wiesendanger, R.; Werner, H.; Schlogl, R.; Zahab, A.; Bernier, P.; Gerth, G.; Anselmetti, D.; Guntherodt, H. J. Appl Phys A 1993, 56, 197.
23. Rashin, A. A.; Honig, B. J Phys Chem 1985, 89, 5588.
24. Hale, J. M. Molecular Dynamic Simulation; Wiley-Interscience: New York, 1992.
25. Rapaport, D. C. The Art of Molecular Dynamics Simulations; Cambridge University Press: Cambridge, England, 1997.
26. Lambin, P.; Senet, P. Int J Quantum Chem 1993, 46, 101.